Materials Chemistry and Physics 157 (2015) 124–129

Contents lists available at ScienceDirect

Materials Chemistry and Physics

journal homepage: www.elsevier.com/locate/matchemphys

Sr hexaferrite/Ni ferrite nanocomposites: Magnetic behavior and microwave absorbing properties in the X-band

Silvia E. Jacobo [a], Paula G. Bercoff [b, *], Carlos A. Herme [a], Leandro A. Vives [c]

[a] Facultad de Ingeniería, Universidad de Buenos Aires, LAFMACEL-INTECIN, Paseo Colón 850, C1063EHA Buenos Aires, Argentina
[b] Facultad de Matemática, Astronomía y Física, Universidad Nacional de Córdoba, IFEG, CONICET, Ciudad Universitaria, X5000HUA Córdoba, Argentina
[c] División Antenas, Instituto de Investigaciones Científicas para la Defensa CITEDEF, Ministerio de Defensa, San Juan Bautista de La Salle 4397, Villa Martelli, B1603ALO Buenos Aires, Argentina

HIGHLIGHTS

- $Sr_{0.5}Co_{0.5}Nd_{0.5}Fe_{10.5}O_{19}/NiFe_2O_4$ nanocomposites were synthesized at different mass ratios.
- The systems were structurally and magnetically characterized.
- The X-band microwave radiation of the composites was evaluated.
- Enhancement in reflectivity is related to exchange interaction between hard and soft phases.

ARTICLE INFO

Article history:
Received 2 September 2014
Received in revised form
2 March 2015
Accepted 12 March 2015
Available online 17 March 2015

Keywords:
Composite materials
Magnetic materials
Nanostructures
Microwave absorption

ABSTRACT

Nickel ferrite nanoparticles were synthesized by a self-combustion method over nanocrystalline powders of Nd–Co substituted strontium hexaferrite with nominal composition $Sr_{0.5}Nd_{0.5}Co_{0.5}Fe_{10.5}O_{19}$, at different mass relations. The samples were structurally characterized by X-ray diffractometry (XRD), scanning electron microscopy (SEM), and energy dispersive X-ray analysis (EDX). The *M vs. H* loops of the composites were determined with a vibrating sample magnetometer (VSM) and the interaction with the X-band microwave radiation of the nanocomposites dispersed in epoxy resin was measured with a vector network analyzer (VNA). The hysteresis loops showed strong exchange-coupling between the two magnetic phases for the 30:70 and 50:50 $Sr_{0.5}Co_{0.5}Nd_{0.5}Fe_{10.5}O_{19}/NiFe_2O_4$ nanocomposites, while a weak interaction was observed for the 70:30 mass ratio. The nanocomposite with an equal amount of hard and soft phase shows the highest performance both in reflectivity and in bandwidth, reaching a maximum in reflectivity of −34.4 dB at 11.1 GHz while the bandwidth below −10 dB is 3.5 GHz.

1. Introduction

The development of microwave absorbing composite materials has gained great interest in the last decades, not only for the problems caused by electromagnetic interference over wireless communications, but also for their use as essential components of stealth defense systems for military purposes [1]. Therefore, extensive research on electromagnetic reflection and absorption properties of many types of materials has been carried out in order to find efficient absorbers over a wide band at the microwave range.

The M-type strontium hexaferrite is a hard ferrimagnetic material, which shows intense absorption peaks above 20 GHz. Hexaferrite materials are suitable as microwave absorbers due to their appropriate permeability values, high magnetization and planar anisotropic behavior in microwave frequencies [2,3]. Due to their high anisotropy field, hexaferrites can be used at much higher frequencies than spinel ferrites or garnets [4–7].

Much research about the influence of lantanide substitution on magnetic and microwave absorption properties of these ferrites has been carried out [8,9]. Besides, many efforts are being made in order to improve their magnetic capabilities by using different synthesis methods [10], including new processes to prepare nano-sized single-domain particles [11]. Substitution for the Fe^{3+} and Sr^{2+} ions in this hexaferrite with Nd^{3+} and Co^{2+} distorts the lattice parameters of its structure, increasing the coercivity of this hard material [12].

* Corresponding author.
E-mail address: bercoff@famaf.unc.edu.ar (P.G. Bercoff).

http://dx.doi.org/10.1016/j.matchemphys.2015.03.026
0254-0584/

Several researchers have addressed the challenge of finding a radar-frequency absorbing material with wide frequency bandwidth [13–15]. Since materials based only on hexaferrites cannot fulfill these demands, multilayer structures were explored in order to combine hexaferrites with other materials having different resonant frequencies [5,16] and new systems of composite powders including hard and soft materials have been developed [17–21]. The reported results correspond to samples where both phases are simultaneously grown, such as $SrFe_{12}O_{19}/\alpha$-Fe_2O_3, $CoFe_2O_4/ZnFe_2O_4$, $BaFe_{12}O_{19}/Ni_{0.8}Zn_{0.2}Fe_2O_4$, $BaFe_{12}O_{19}/Fe_3O_4$ [17,22–24].

In this work, hard-soft $Sr_{0.5}Co_{0.5}Nd_{0.5}Fe_{10.5}O_{19}/NiFe_2O_4$ nanocomposites were prepared in a two-step self-combustion method. Self-combustion is a unique combination of the combustion and the chemical gelation processes. This method exploits the advantages of cheap precursors, simple preparation, atomic-level diffusion and a resulting ultra-fine and homogeneous powder. An iron deficient Nd–Co strontium hexaferrite $Sr_{0.5}Co_{0.5}Nd_{0.5}Fe_{10.5}O_{19}$ was chosen as a hard phase (first step) [12,25] and nickel ferrite (second step) was chosen as soft magnetic phase because of its high magnetization [9]. Nickel ferrite, a soft magnetic material with cubic spinel structure, has significant reflection loss values at lower frequencies (MHz range). The content of soft magnetic phase was systematically varied to study its effect on the overall magnetic properties of the nanocomposite and the electromagnetic response at the microwave X-band when both phases are present.

2. Experimental procedure

2.1. Synthesis of Nd–Co doped Sr hexaferrite (first step)

Nd–Co substituted strontium hexagonal ferrite was prepared by a self-combustion method. Stoichiometric amounts of $Fe(NO_3)_3\cdot 9H_2O$, $SrCO_3$, Nd_2O_3 and $Co(CH_3CO_2)_2\cdot 4H_2O$ were weighed to obtain a doped Sr ferrite with nominal composition $Sr_{0.5}Co_{0.5}Nd_{0.5}Fe_{10.5}O_{19}$. The salts were dissolved in nitric acid, then the solution was neutralized with concentrated ammonia and a citric acid solution was added in order to obtain citrate complexes of the metallic ions. The citrate:nitrate ratio was fixed in 1:1 for each experiment. The pH of this solution was fixed at 8.0 and then it was slowly evaporated until reaching the self ignition of the precipitated gel. The obtained ashes were grinded and heat-treated at 800 °C for 2 h. This sample of doped Sr ferrite was named C10.

2.2. Synthesis of Ni ferrite/Sr hexaferrite composites (second step)

The particles of hexaferrite C10 were suspended by sonication for one hour in an aqueous solution of $Ni(NO_3)_2\cdot 6H_2O$, $Fe(NO_3)_3\cdot 9H_2O$ (with three different cation concentrations) and citric acid at pH 8.0. Then these mixtures were also evaporated up to self ignition. The composite products were gently grinded and heat-treated at 800 °C for 2 h in order to prevent grain size growth.

Three samples of $Sr_{0.5}Co_{0.5}Nd_{0.5}Fe_{10.5}O_{19}/NiFe_2O_4$ with different weight ratios, labeled C37, C55 and C73 were obtained (Table 1). A similar procedure, without any C10 addition was followed to prepare $NiFe_2O_4$ nanoparticles (sample C01).

Table 1
Samples labeling and nominal as well as measured compositions.

Sample	Wt.% Sr hexaferrite (nominal)	Wt.% Ni ferrite (nominal)	Wt.% Sr hexaferrite (EDX)	Wt.% Ni ferrite (EDX)
C10	100	–	100	–
C73	70	30	78	22
C55	55	50	52	48
C37	30	70	35	65
C01	–	100	–	100

2.3. Characterization studies

The thermal stability of the as-prepared gel (Section 2.1) from C10 was analyzed by thermogravimetry (TG) in a DTG50 Shimadzu Thermoanalyzer, heating in nitrogen at 10 K/min from room temperature up to 1100 °C. The structural analysis of the ferrites and composite powders was performed by X-ray diffraction (XRD) using a Philips PW3120 diffractometer and Cu Kα radiation. The diffractograms were taken between $2\theta = 10°$ and 70° with a step of 0.05°. The chemical composition of the nanocomposites was assessed via SEM-EDX, with a Sigma Zeiss microscope, which was also used to take images of the powders.

A vibrating sample magnetometer (VSM) Lakeshore 7300 was used to measure the magnetic properties at room temperature. Hysteresis loops *M vs. H* were measured with a maximum applied field of 15 kOe.

2.4. Preparation of samples for microwave reflection

Grinded powders of the ferrites and their composites were mixed with epoxy resin and a hardener as a filler in order to obtain mixtures sample/resin of about 45 wt%. The mixtures were poured into aluminum sample holders with a rectangular shaped window of 23 × 10 × 4 mm. The samples obtained in this way include a letter "E" after their nomination in order to indicate the epoxy presence (*i.e.* C10-E, etc.).

2.5. Measurement of electromagnetic properties

The samples were measured with an Anritsu Vector Network Analyzer between 7 and 13 GHz. Microwave reflection properties were measured in a rectangular transmission line. The test sample was inserted in the conductor of the coaxial line and then the rear face of the sample was covered by a perfect conductor aluminum plate as a short-circuiter.

The scalar value of reflection voltage was measured using one port of the network analyzer. The power reflectivity can be calculated from the voltage reflectivity using the following relations:

$$\Gamma_V = \frac{V_r}{V_i} = S_{11} \quad (1)$$

$$\Gamma_P = |S_{11}|^2 \quad (2)$$

$$R(f) = 10\log\Gamma_P = 10\log|S_{11}|^2 (dB) \quad (3)$$

where Γ_V is the voltage reflectivity, V_r is the reflection voltage, V_i is the incident voltage, S_{11} is the reflected scattering parameter, Γ_P is the power reflectivity, and R (*f*) is the decibel value of the power reflectivity, which is usually plotted as a function of the frequency *f* in order to have an insight of the absorbing properties.

A power reflectivity of 10 dB, corresponding to 90% attenuation of the EMI (Electromagnetic Interference), is considered an adequate level of shielding for many applications [26].

3. Results and discussion

3.1. Structural characterization

The thermogravimetry (TG) and differential thermal analysis of the as-prepared gel of the hexaferrite (C10) is shown in Fig. 1. TG

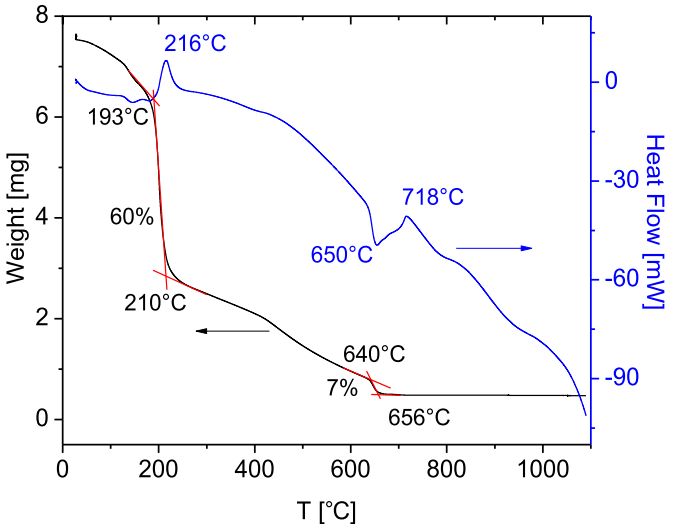

Fig. 1. TG-DTA profiles of the as-prepared $Sr_{0.5}Co_{0.5}Nd_{0.5}Fe_{10.5}O_{19}$ gel.

analysis shows a weight loss of 60% in the temperature range of 193–210 °C which may be due to degassing, loss of moisture and removal of organic products (citric acid) during the heating. This mass decrease is accompanied by an exothermic peak in the DTA profile (216 °C). After a slight mass decrease (7%) between 640 °C and 656 °C it can be considered that the hexaferrite phase is completely formed as the exothermic peak at 718 °C occurs at constant mass. This fact is confirmed by XRD results (Fig. 2).

XRD profiles of all the prepared samples are shown in Fig. 2. All the powder samples can be indexed with either $Sr_{0.5}Co_{0.5}Nd_{0.5}Fe_{10.5}O_{19}$ (C10) (033-1340-P6/mmm) and/or $NiFe_2O_4$ (C01) (074-1913-Fd/3m). According to JCPDS Card No. 33-0664, some hematite (α-Fe_2O_3) is also formed besides the hexaferrite. The diffractograms that correspond to the composites show the main reflections of the magnetoplumbite structure and a spinel phase. In samples with a hexaferrite/spinel mass ratio H/S $\leq$ 1 (samples C55 and C37) the intensity of the hexaferrite peaks are diminished, indicating that possibly the soft phase is covering the hard phase. This is not

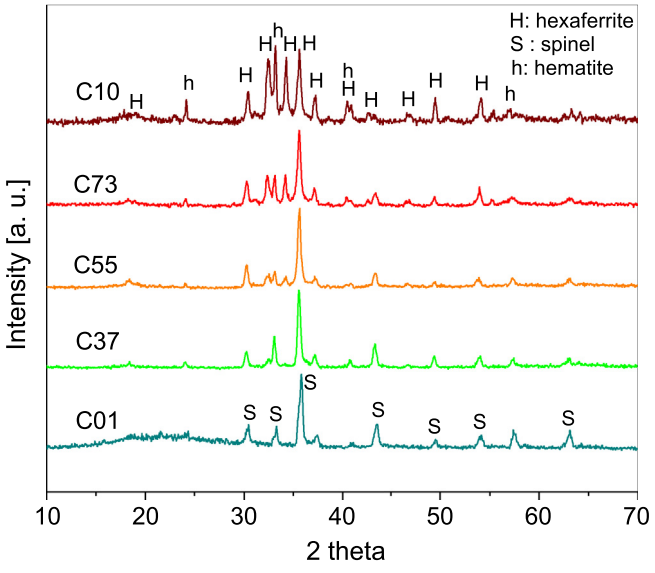

Fig. 2. XRD of $Sr_{0.5}Co_{0.5}Nd_{0.5}Fe_{10.5}O_{19}/NiFe_2O_4$. Hexaferrite (C10) and spinel phase (C01) are included for comparison. Hematite (h) appears as secondary phase.

observed in sample C73, where both phases are noticed.

The average crystallite sizes, calculated using Scherrer's formula, are about 35 nm for $Sr_{0.5}Co_{0.5}Nd_{0.5}Fe_{10.5}O_{19}$ and 30 nm for $NiFe_2O_4$.

In order to confirm the chemical composition of the $Sr_{0.5}Co_{0.5}Nd_{0.5}Fe_{10.5}O_{19}/NiFe_2O_4$ nanocomposites, a quantitative elemental analysis on these samples was performed using SEM-EDX (not shown). The measured compositions of the nanocomposites are listed in Table 1, showing good agreement with the nominal values.

Fig. 3 shows the morphology of $Sr_{0.5}Co_{0.5}Nd_{0.5}Fe_{10.5}O_{19}/NiFe_2O_4$ nanocomposites (C55 and C73) in a) and b) respectively. The hexagonal phase shows plate shaped particles (Fig. 3c) while the spinel phase shows cubic shaped particles (Fig. 3d). The hexagonal faces of the grains observed in this image correspond to the (111) planes of the fcc crystalline structure. Mainly cubic nanoparticles, corresponding to Ni ferrite, can be observed in sample C55 (Fig. 3a) probably as a consequence of the preparation method where the soft phase was synthesized over the hard nanoparticles. This observation agrees with XRD results for this sample. Larger hexagonal particles are visible in sample C73 (right top corner of Fig. 3b) because in this sample H/S > 1.

3.2. Magnetic characterization

The room temperature hysteresis loops *M vs. H* measured for all the composites are shown in Fig. 4 (the inset displays the corresponding to Ni ferrite) while the corresponding values of maximum magnetization M_{max}, coercivity H_C and remanence *Mr* are listed in Table 2.

The hysteresis loop of sample C10 corresponds to a hard magnetic material, with coercivity of 4.52 kOe. The low-temperature thermal treatment, as well as the presence of hematite as a secondary phase in the formation of $Sr_{0.5}Co_{0.5}Nd_{0.5}Fe_{10.5}O_{19}$ can be the responsible for the reduction in its magnetization. It was previously reported [12] that when calcining $Sr_{0.5}Co_{0.5}Nd_{0.5}Fe_{10.5}O_{19}$ at 1100 °C for two hours, a value of $M_S = 65$ emu/g is measured.

As it can be seen in Fig. 4, when comparing the hexaferrite/spinel composites with sample C10 (pure hexaferrite) there is a reduction in the coercive field (H_C).

Sample C73 displays the typical curve of a hard-soft mixture, not completely exchange-coupled, showing a typical two loop "bee waist"-type hysteresis loop [23], suggesting an incomplete exchange-coupling between the hard and soft phases [27]. Samples C55 and C37, however, show a single-phase magnetic behavior, with smooth hysteresis loops, indicating effective interphase exchage-coupling, which results in cooperative magnetization inversion of the two phases. This observation can be confirmed by studying the switching field distribution, represented by the d*M*/d*H vs. H* curve (Fig. 5).

Magnetic susceptibility $\chi = dM/dH$ is often computed to evaluate the magnetic interaction in different systems, since this magnitude is related to the switching or inversion field distribution. The maximum in d*M*/d*H* coincides with coercivity H_C in systems with a single magnetic phase and an unimodal inversion-field distribution.

The susceptibility χ was calculated as the derivative of *M* with respect to *H* of the upper branch of the hysteresis loop and is shown in Fig. 5 for the composites, as well as for the single Sr (C10) and Ni (C01) ferrites.

As expected for a single magnetic phase, sample C01 displays a single peak centered at 0.28 kOe, close to the measured coercivity of 0.12 kOe (Table 2), indicating a rather narrow particle size distribution. For sample C10, a wide inversion field distribution centered at 6.59 kOe is observed. This behavior has been already reported in similar samples prepared by the same method [12]

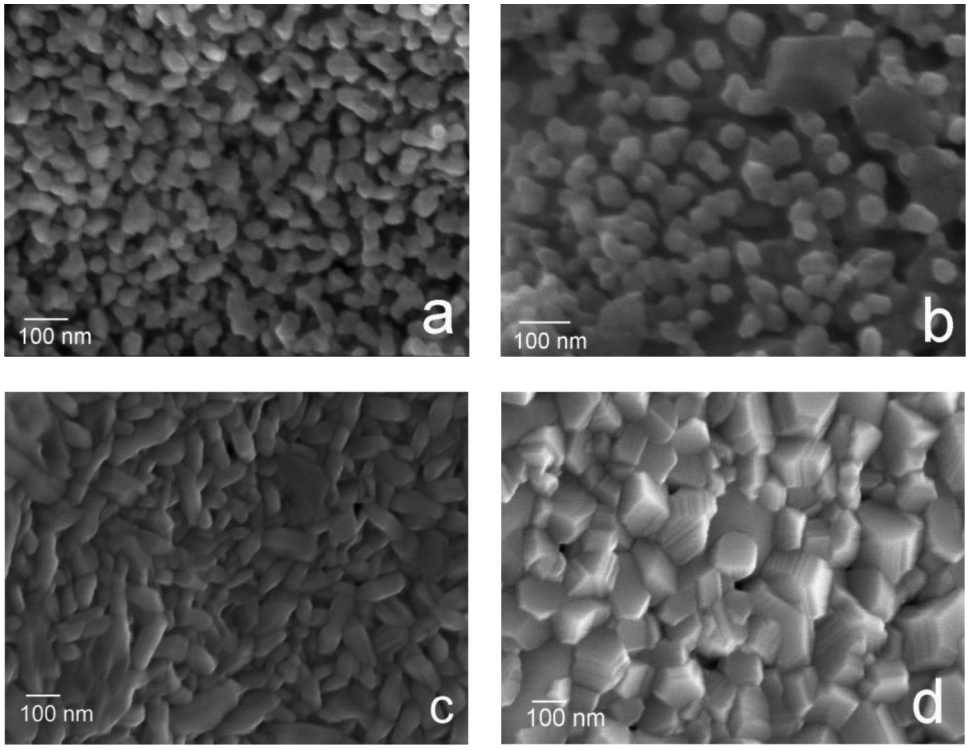

Fig. 3. SEM images of $Sr_{0.5}Co_{0.5}Nd_{0.5}Fe_{10.5}O_{19}/NiFe_2O_4$ composites: C55 (a), C73 (b). Single phase hexaferrite C10 (c) and Ni ferrite C01 (d).

where this effect was explained with the existence of inhomogeneous magnetic orderings.

The hard-soft composites show a particular behavior. Two different peaks can be observed in sample C73 centered at 0.46 kOe and 5.12 kOe corresponding to the soft and hard phases respectively, indicating a very weak coupling between them. The magnetic moments of the interface between the hexaferrite and Ni ferrite deviate from the local axis and arrange parallel with each other, which leads to a higher value of magnetization than C10. However, at this composition a large part inside both hard and soft grains could remain uncoupled [21].

However, for samples C55 and C37, a single peak can be observed in dM/dH (0.39 kOe and 0.45 kOe, respectively), associated with a complete exchange coupling between both phases. These values are larger than the corresponding to the soft phase alone. A possible explanation for such a strong exchange coupling is the characteristics of the two-step method used for the preparation of these samples. The soft phase growth occurs through the nucleation-and-growth mechanism on top of the hexaferrite nanoparticles, enhancing the interfacial exchange coupling between both phases.

Other researchers studied similar composites prepared by simultaneous co-precipitation of hard and soft ferrites [18,22,27]. They reported a partial exchange coupling between both phases through the interface of ferrite particles, promoted by the similarity of the spinel crystal structure of Ni ferrite to the S-block structure of the hexaferrite. The magnitude of this interaction is highly related to particle size as there will be more interfaces if the grain size is smaller. Rai et al. [21] argued that the exchange-coupling interaction in similar hard-soft nanocomposites occurs within the exchange-length $\delta_{ex} = (A\,K_1)^{1/2}$ (~8 nm for Ba hexaferrite [28]) and there is no exchange-coupling in the inner part of the grains.

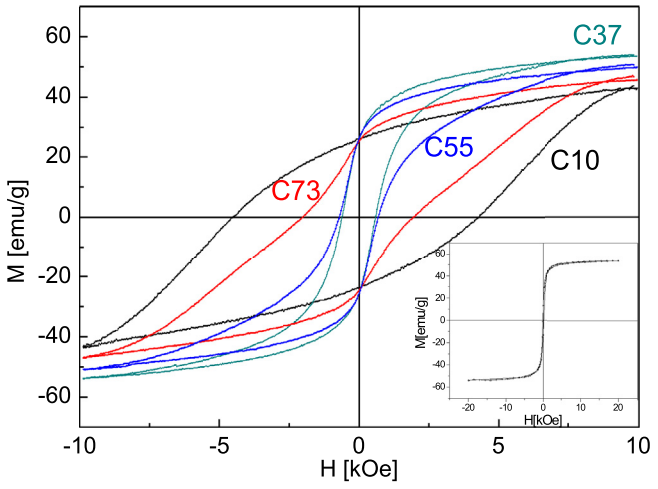

Fig. 4. Hysteresis loops of the studied samples. The inset shows the corresponding to Ni ferrite.

3.3. Microwave characterization

Fig. 6 shows the frequency dependence of the powder reflectivity (dB) of the samples immersed in epoxy-resin in the X-band

Table 2
Maximum magnetization at 15 kOe M_{max}, remanence Mr and coercivity H_C of $Sr_{0.5}Co_{0.5}Nd_{0.5}Fe_{10.5}O_{19}/NiFe_2O_4$ composites.

Sample	M_{max} [emu/g]	Mr [emu/g]	H_C [kOe]
C10	42.7	26.0	4.52
C73	45.7	25.2	2.03
C55	49.9	26.3	0.72
C37	53.5	27.8	0.60
C01	57.6	12.7	0.12

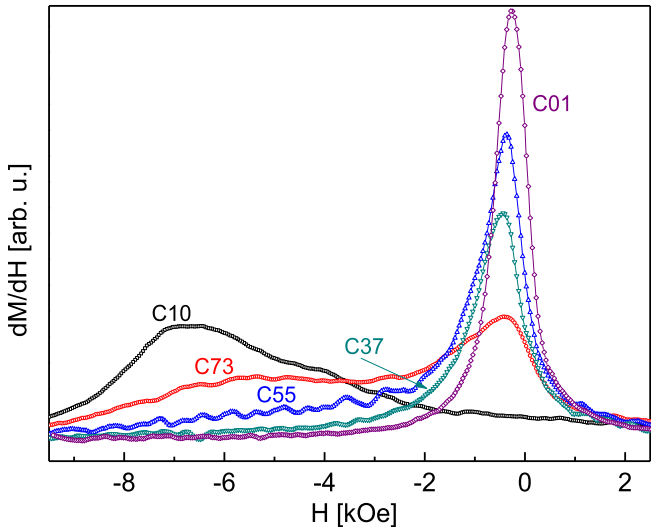

Fig. 5. Switching field distribution d*M*/d*H* for all the studied samples.

range. In this figure, a horizontal dashed line indicates the minimum reflectivity which is adequate for shielding applications.

As expected for Ni ferrite (C01-E) there is no significant absorption in the explored frequency range. On the other hand, the single hexaferrite (C10-E) has a wide absorption band of 1 GHz starting at 8.8 GHz. This behavior can be explained considering two main contributions. Generally, microwave magnetic losses of magnetic particles originate from hysteresis, domain wall resonance, eddy currents, and ferromagnetic resonance. In this case, the hysteresis loss is negligible in the weak field associated to the EM wave. The domain wall displacement loss occurs only in the MHz range rather than that of GHz; on the other hand these hexaferrite particles are single domain (<1 μm). Therefore, the contribution of domain wall resonance can also be excluded. The eddy currents loss, which is related to the thickness and electric conductivity, can be ignored (ferrites are nonconductive). Therefore, the only contributions to microwave absorption in this sample come from the decrease in coercivity due to the high Nd–Co substitution and from the nanometric particles obtained after the low temperature, short thermal treatment (800 °C for 2 h), which increases the superficial area. As a consequence of a smaller particle size, interface

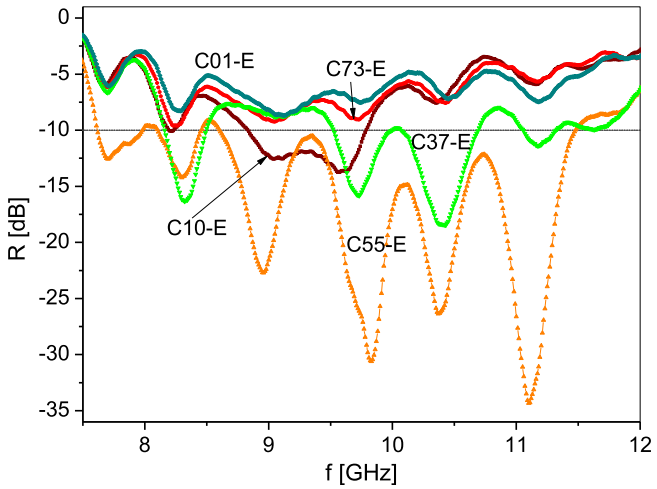

Fig. 6. Reflectivity *R*(*f*) of the studied samples. The dashed line at 10 dB indicates the minimum value adequate for shielding applications.

polarization and multiple scatter become important factors for the attenuation [20]. S. Ruan et al. reported the preparation of a nanocrystalline composite material as microwave absorber [29], showing an important increase in the reflection loss of Zn–Co substituted Ba hexaferrite when reducing from micro to nano-sized particles.

The reflectivity response of the different composites, shown in Fig. 6, is closely related to the H/S ratio. For C73-E a negligible change with respect to C01-E is observed despite the high hexaferrite content of this sample. On the other hand, an important enhancement in the reflectivity is observed for samples C55-E and C37-E. Sample C55-E reaches a maximum in reflectivity of −34.4 dB at 11.1 GHz while the bandwidth below −10 dB is 3.5 GHz (Table 3). Sample C37-E reaches −18.5 dB at 10.4 GHz, with a narrower bandwidth of 1.2 GHz (Table 3).

The improvement of reflectivity in these composites can be explained on the basis of exchange coupling interaction between the hard and soft magnetic phases and the decrease of coercivity (Table 2). In general, reflectivity *R* is increased by a decrease in coercivity and an increase in magnetization. Thus, changes in *R* (Fig. 6) can be explained due to the decrease in H_C and the increase in M_{max} observed for hexaferrite particles as the exchange interaction with the spinel phase increases (Table 2). The appearance of multiple peaks in the reflectivity profile of C55-E and C37-E is related to the nanoscale of these systems and the particle size distributions [30].

Since the reflectivity profiles display multiple peaks, a fixed frequency of 9.8 GHz was chosen in order to compare the absorption values of all the studied samples. Table 3 shows that both composites C37-E and C55-E have improved their reflectivity when comparing with the single-phase ferrites as a consequence of the exchange coupling interaction existing between the hard and soft magnetic phases (interface effect). Tyagi et al. [18] reported the electromagnetic properties of a composite of nickel and zinc substituted strontium hexaferrite, $SrFe_{11}Zn_{0.5}Ni_{0.5}O_{19}$ ($SrFe_{12}O_{19}$/$NiFe_2O_4$/$ZnFe_2O_4$) nanoparticles synthesized by co-precipitation and heat-treated at 900 °C and 1200 °C for 4 h in nitrogen atmosphere. They reported a maximum reflection loss of 29.62 dB (99% power attenuation) at 10.21 GHz for the material calcined at 1200 °C. This co-precipitation method was also employed by Mehdipour et al. [20] for the preparation of a ferromagnetic system ($SrFe_{12}O_{19}$/$NiFe_2O_4$) of nanostructured particles. They reported that the maximum microwave loss reaches 18 dB at 11 GHz, and a bandwidth with the loss above 10 dB is about 0.5 GHz in the 10.7–11.2 GHz range. Our results are clearly comparable to these ones (and ever better to some) with the advantage that the proposed synthesis method is simple, low-cost, fast and easily implementable in the large scale. Sample C55-E has the highest performance both in bandwidth and in reflectivity, reaching 30.7 dB in the 8–11.5 GHz range.

4. Conclusions

In this work, hard-soft $Sr_{0.5}Co_{0.5}Nd_{0.5}Fe_{10.5}O_{19}$/$NiFe_2O_4$ nanocomposites were successfully prepared in a two-step method by

Table 3
Reflectivity properties of the studied samples.

Sample	Frequency range [GHz] (>10 dB)	*R* (*f* = 9.8 GHz) [dB]
C10-E	–	−10
C73-E	–	−8.3
C55-E	8–11.5	−30.7
C37-E	9.5–10.7	−14
C01-E	–	−7.2

self-combustion at low temperature. Different hard/soft ratios were explored. SEM images indicate nanometric particle size distributions for all the samples.

When the amount of soft phase is equal or larger than the amount of hard phase, the soft phase grows on top of the hexagonal nanoparticles of Sr hexaferrite. For H/S $\leq$ 1, the nanocomposites C55-E and C37-E show a single-phase-like magnetic behavior with smooth demagnetizing curves, indicating effective interphase exchange-coupling, which results in cooperative magnetization switching of the two phases. This coupling improves these samples' reflectivity. The nanocomposite with an equal amount of hard and soft phase, shows the highest performance both in bandwidth and in reflectivity. Besides having a very good response for microwave absorption, this system has the advantage of a simple synthesis method, which is also low-cost, fast and easily implementable in the large scale.

Hard-soft $Sr_{0.5}Co_{0.5}Nd_{0.5}Fe_{10.5}O_{19}/NiFe_2O_4$ nanocomposites open up the possibility of controlling the microwave operating frequency of these materials by varying the H/S compositions.

Acknowledgments

This work was partially funded by UBACyT, Secyt-UNC and CONICET. The authors thank CITEDEF for the use of the Network Analyzer and LAMARX for the use of the SEM-EDX.

References

[1] V.G. Harris, Modern microwave ferrites, IEEE Trans. Magn. 48 (3) (2012) 1075–1104.
[2] M.B. Amin, J.R. James, Techniques for utilization of hexagonal ferrites in radar absorbers part 1 broadband planar coatings, Radio Electron. Eng. 51 (5) (1981) 209–218.
[3] I. Nedkov, A. Petkov, V. Karpov, Microwave absorption in Sc- and CoTi-substituted Ba hexaferrite powders, IEEE Trans. Magn. 26 (5) (1990) 1483–1484.
[4] Y. Feng, T. Qiu, C. Shen, X. Li, Complex permeability and permittivity and microwave absorption property of barium ferrite/EPDM rubber radar absorbing materials in 2–18 GHz, in: IEEE APMC2005 Proc., 2005.
[5] J. Qiu, M. Gu, H. Shen, Microwave absorption properties of Al- and Cr-substituted M-type barium hexaferrite, J. Magn. Magn. Mater. 295 (3) (2005) 263–268.
[6] A. Ghasemi, A. Saatchi, M. Salehi, A. Hossienpour, A. Morisako, X. Liu, Influence of matching thickness on the absorption properties of doped barium ferrites at microwave frequencies, Phys. Stat. Sol. (A) 203 (2) (2006) 358–365.
[7] E. Kiani, A.S.H. Rozatian, M.H. Yousefi, Structural, magnetic and microwave absorption properties of $SrFe_{12-2x}(Mn_{0.5}Cd_{0.5}Zr)_xO_{19}$ ferrite, J. Magn. Magn. Mater. 361 (2014) 25–29.
[8] R. Grössinger, M. Küpferling, J.C. Tellez Blanco, G. Wiesinger, M. Müller, G. Hilscher, M.W. Pieper, J.F. Wang, I.R. Harris, Rare earth substitutions in M-type ferrites, IEEE Trans. Magn. 39 (5) (2003) 2911–2913.
[9] S.E. Jacobo, S. Duhalde, H.R. Bertorello, Rare earth influence on the structural and magnetic properties of NiZn ferrites, J. Magn. Magn. Mater. 272–276 (3) (2004) 2253–2254.
[10] R.C. Pullar, Hexagonal ferrites: a review of the synthesis, properties and applications of hexaferrite ceramics, Prog. Mater. Sci. 57 (2012) 1191–1334.
[11] T. Inui, N. Ogasawara, Grain-size effects on microwave ferrite magnetic properties, IEEE Trans. Magn. 13 (6) (1977) 1729–1744.
[12] C.A. Herme, P.G. Bercoff, S.E. Jacobo, Nd-Co substituted strontium hexaferrite powders with enhanced coercivity, Mat. Res. Bull. 47 (2012) 3881–3887.
[13] H. Zhao, X. Sun, C. Mao, J. Du, Preparation and microwave-absorbing properties of $NiFe_2O_4$-polystyrene composites, Phys. B 404 (2009) 69–72.
[14] Z. Zhang, X. Liu, X. Wang, Y. Wu, R. Li, Effect of Nd-Co substitution on magnetic and microwave absorption properties of $SrFe_{12}O_{19}$ hexaferrites, J. Alloys Compd. 525 (2012) 114–119.
[15] Z. Peng, J. Hwang, M. Andriese, Microwave power absorption characteristics of ferrites, IEEE Trans. Magn. 49 (3) (2013) 1163–1166.
[16] B. Li, Y. Shen, Z. Yue, C. Nan, Enhanced microwave absorption in nickel/hexagonal-ferrite/polymer composites, Appl. Phys. Lett. 89 (13) (2006) 132504, http://dx.doi.org/10.1063/1.2357565.
[17] C. Fei, Y. Zhang, Z. Yang, Y. Liu, R. Xiong, J. Shi, X. Ruan, Synthesis and magnetic properties of hard magnetic ($CoFe_2O_4$)-soft magnetic (Fe_3O_4) nano-composite ceramics by SPS technology, J. Magn. Magn. Mater. 323 (13) (2011) 1811–1816.
[18] S. Tyagi, H.B. Baskey, R.C. Agarwala, V. Agarwala, T.C. Shami, Development of hard/soft ferrite nanocomposite for enhanced microwave absorption, Ceram. Int. 37 (2011) 2631–2641.
[19] C.A. Herme, P.G. Bercoff, S.E. Jacobo, Formation of a magnetic composite by reduction of Co-Nd doped strontium hexaferrite in a hydrogen gas flow, Phys. B 407 (2012) 3102–3105.
[20] M. Mehdipour, H. Shokrollahi, Comparison of microwave absorption properties of $SrFe_{12}O_{19}$, $SrFe_{12}O_{19}/NiFe_2O_4$, and $NiFe_2O_4$ particles, J. Appl. Phys. 114 (4) (2013) 043906, http://dx.doi.org/10.1063/1.4816089.
[21] B.K. Rai, L. Wang, S.R. Mishra, V.V. Nguyen, J.P. Liu, Synthesis and magnetic properties of hard-soft $SrFe_{10}Al_2O_{19}/NiZnFe_2O_4$ ferrite nanocomposites, J. Nanosci. Nanotechnol. 14 (2014) 5272–5277.
[22] X. Liu, W. Zhong, B. Gu, Y. Du, Exchange-coupling interaction in nanocomposite $SrFe_{12}O_{19}/\gamma$-Fe_2O_3 permanent ferrites, J. Appl. Phys. 92 (2) (2002) 1028–1032.
[23] Y. Wang, Y. Huang, Q. Wang, Preparation and magnetic properties of $BaFe_{12}O_{19}/Ni_{0.8}Zn_{0.2}Fe_2O_4$ nanocomposite ferrite, J. Magn. Magn. Mater. 324 (19) (2012) 3024–3028.
[24] P.G. Bercoff, H.R. Bertorello, High-energy ball milling of Ba-hexaferrite/Fe magnetic composite, J. Magn. Magn. Mater. 187 (2) (1998) 169–176.
[25] S.E. Jacobo, C. Herme, P.G. Bercoff, Influence of the iron content on the formation process of substituted Co-Nd strontium hexaferrite prepared by the citrate precursor method, J. Alloys Compd. 495 (2010) 513–515.
[26] S. Yang, K. Lozano, A. Lomeli, H.D. Foltz, R. Jones, Electromagnetic interference shielding effectiveness of carbon nanofiber/LCP composites, Compos. Part A 36 (2005) 691–697.
[27] S. Hazra, M.K. Patra, S.R. Vadera, N.N. Ghosh, A novel but simple "One-Pot" synthetic route for preparation of $(NiFe_2O_4)_x$–$(BaFe_{12}O_{19})_{1-x}$ composites, J. Am. Ceram. Soc. 95 (1) (2012) 60–63, http://dx.doi.org/10.1111/j.1551-2916.2011.04958.x.
[28] G. Bertotti, Hysteresis in Magnetism, Academic Press, 1998.
[29] Shengping Ruan, Baokun Xu, Hui Suo, Fengqing Wu, Siqing Xiang, Muyu Zhao, Microwave absorptive behavior of ZnCo-substituted W-type Ba hexaferrite nanocrystalline composite material, J. Magn. Magn. Mater. 212 (2000) 175–177.
[30] Z.W. Liu, D.C. Zeng, R.V. Ramanujan, X.C. Zhong, H.A. Davies, Exchange interaction in rapidly solidified nanocrystalline RE–(Fe/Co)–B hard magnetic alloys, J. Appl. Phys. 105 (7) (2009), 07A736-07A739.